The nature of the charge-ordered state in $Y_{0.5}Ca_{0.5}MnO_3$ with a very small average radius of the A-site cations

1998 J. Phys.: Condens. Matter 10 4447

(http://iopscience.iop.org/0953-8984/10/20/012)

J. Phys.: Condens. Matter **10** (1998) 4447–4456. Printed in the UK PII: S0953-8984(98)90914-6

The nature of the charge-ordered state in $Y_{0.5}Ca_{0.5}MnO_3$ with a very small average radius of the A-site cations

Anthony Arulraj†, R Gundakaram†, Amlan Biswas‡, N Gayathri‡, A K Raychaudhuri‡ and C N R Rao†§

† Solid State and Structural Chemistry Unit, Indian Institute of Science, Bangalore 560 012, India

‡ Department of Physics, Indian Institute of Science, Bangalore 560 012, India

Received 21 January 1998

Abstract. A detailed investigation of $Y_{0.5}Ca_{0.5}MnO_3$ with a very small radius of the A-site cations ($\langle r_A \rangle \approx 1.13$ Å) reveals the occurrence of a charge-ordering transition in the paramagnetic state, at a relatively high temperature of 260 K. The orthorhombic lattice distortion, as measured by the dimensionless index D, is large (∼1.75%) over the entire 300–100 K range, but the antiferromagnetic interactions become prominent only at low temperatures (<160 K). The charge-ordering gap in $Y_{0.5}Ca_{0.5}MnO_3$, measured by low-temperature vacuum tunnelling spectroscopy, is large (∼0.5 eV) and the charge-ordered state is unaffected by the application of a magnetic field of 6 T. The study indicates that the nature of charge-ordering in $Y_{0.5}Ca_{0.5}MnO_3$ which is dominated by the cooperative Jahn–Teller effect and the associated lattice distortion is distinctly different from analogous manganates with larger $\langle r_A \rangle$.

1. Introduction

Studies of colossal magnetoresistance (CMR) and related properties of rare-earth manganates of the type $Ln_{1-x}A_xMnO_3$ (Ln = rare earth, A = alkaline earth) have revealed certain interesting aspects of charge and spin dynamics in these solids [1, 2]. These properties of the manganates cannot be fully understood without taking into account electron–phonon coupling [3, 4]. Important lattice effects arise due to charge-ordering of Mn^{3+} and Mn^{4+} ions which is favoured when the concentration of the two are comparable. Charge-ordering in the manganates is strongly affected by the average radius of the A-site cation, $\langle r_A \rangle$. A small $\langle r_A \rangle$ gives rise to a significant deviation of the Mn–O–Mn bond angle from 180° and hence decreases the one-electron e_g bandwidth. The qualitative phase diagram in figure 1, constructed on the basis of recent studies of rare-earth manganates, shows how $\langle r_A \rangle$ affects charge-ordering in these materials. The diagram shows that when $\langle r_A \rangle$ is large (in region A), the ferromagnetic metallic state is stable. Such manganates do not show charge-ordering (e.g., $La_{0.7}Sr_{0.3}MnO_3$ with $\langle r_A \rangle$ of 1.244 Å). With a slightly smaller $\langle r_A \rangle$, the ferromagnetic state becomes unstable and transforms to an antiferromagnetic charge-ordered (CO) state on cooling as in the region B of the figure (e.g. $Nd_{0.5}Sr_{0.5}MnO_3$ with $\langle r_A \rangle$ of 1.236 Å) [5]. When $\langle r_A \rangle$ is very small, as in region D, the oxide does not exhibit ferromagnetism and gives rise to a insulating charge-ordered ground state (e.g. $Pr_{0.7}Ca_{0.3}MnO_3$ with $\langle r_A \rangle$ of 1.179) [6, 7]. Since charge-ordering depends on the extent of Coulomb interaction, one

§ For correspondence: cnrrao@sscu.iisc.ernet.in

0953-8984/98/204447+10$19.50

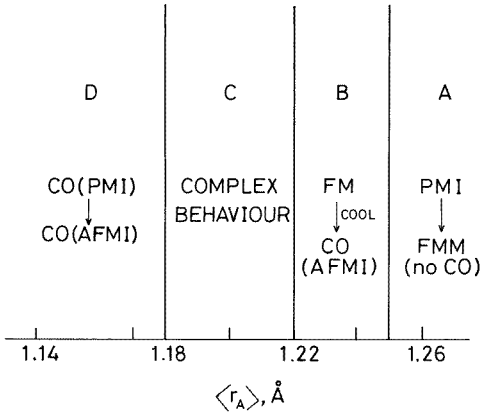

Figure 1. Schematic phase diagram of rare-earth manganates showing different types of charge-ordering effect with the variation in the average radius of the A-site cations. FMM, ferromagnetic metal; PMI, paramagnetic insulator; AFMI, antiferromagnetic insulator; CO, charge-ordered state.

would expect that the CO state obtained from a metallic state and from a charge localized state will have different scales of CO energy. The CO transition from a charge localized state would not be sharp, but manifests itself as a change in the slope of the resistivity–temperature plots [6, 8, 9].

Charge-ordered states in the manganates of the general composition $Ln_{0.5}A_{0.5}MnO_3$ are generally transformed ('melted') to the metallic state by the application of magnetic fields [1, 2]. It was our interest to investigate how the stability of the charge-ordered state against magnetic fields depends on $\langle r_A \rangle$. We have therefore carefully investigated the properties of $Y_{0.5}Ca_{0.5}MnO_3$ with the smallest $\langle r_A \rangle$ value examined hitherto (1.128 Å). We find that it exhibits distinct features arising from charge-ordering in the electrical, magnetic and other properties. The lattice shows a strong orthorhombic distortion which increases with decrease in temperature. More interestingly, it is not possible to melt the charge-ordered state in $Y_{0.5}Ca_{0.5}MnO_3$ by the application of magnetic fields up to 6 T. We demonstrate that this arises from the large charge-ordering gap in $Y_{0.5}Ca_{0.5}MnO_3$ as measured by low temperature scanning tunnelling microscopy.

2. Experimental details

Polycrystalline samples of $Y_{0.5}Ca_{0.5}MnO_3$ were prepared by heating stoichiometric proportions of Y_2O_3, $CaCO_3$ and freshly precipitated $MnCO_3$ at 1673 K for 12 hours in air. The mixture so obtained was ground thoroughly, pelletized and heated in air at 1673 K for 12 hours. This procedure was repeated twice. The exact Mn^{4+} content was found to be 43% by redox titrations, using standard potassium permanganate and ferrous sulphate solutions. The phase purity was tested by x-ray diffraction patterns and EDAX analysis. A STOE/STADIP high resolution x-ray diffractometer was employed for determining the unit cell parameters.

Magnetic susceptibility and magnetization measurements were carried out with a constant field gradient provided by a pair of Lewis coils. The data were taken at different applied fields. Magnetization was measured in the field-cooled (FC) and zero-field-cooled (ZFC) mode. The resistivity and magnetoresistance were measured in an He cryostat using

a superconducting solenoid. EPR line widths were obtained from the spectra recorded with a Varian E-109 X-band spectrometer. Scanning tunnelling spectroscopy employed to determine the CO gap was carried out in a cryo-pumped vacuum environment. The sample was baked to 375 K in high vacuum before the data were recorded. The details of the technique used are available elsewhere [10, 11].

3. Results and discussion

The x-ray diffraction pattern of $Y_{0.5}Ca_{0.5}MnO_3$ could be indexed on an orthorhombic cell with $a = 5.305$ Å, $b = 5.495$ Å and $c = 7.445$ Å. The structure is therefore of the O′ type with $c\sqrt{2} < a < b$, resulting from the small value of $\langle r_A \rangle$. The electrical resistivity of $Y_{0.5}Ca_{0.5}MnO_3$ as a function of temperature is presented in figure 2. The resistivity is relatively small around 300 K ($\rho_{300} \approx 1.4$ ohm cm), but rises rapidly on cooling. At the lowest temperature measured ($T \approx 100$ K), the resistivity is in excess of 10^4 ohm cm (see inset of figure 2). A charge-ordering transition in manganates is often seen as a change in the local slope in resistivity. We find such a change in the plot of the logarithmic derivative $\delta = \mathrm{d}(\log \rho)/\mathrm{d}(T^{-1})$ against temperature as presented in figure 3. The plot shows a change in the slope as a peak in δ around 260 K which we attribute to the charge-ordering transition. A similar change in slope has been seen in charge-ordered systems such as $La_{0.35}Ca_{0.65}MnO_3$ ($T_{CO} \approx 265$ K) [8], $Pr_{1-x}Ca_xMnO_3$ (for $0.4 \leqslant \chi \leqslant 0.7$ with $T_{CO} \approx 200$ K) [6] and $Nd_{0.5}Ca_{0.5}MnO_3$ ($T_{CO} \approx 200$ K) [9] which undergo transitions to a CO state from an insulating state. At $T \ll T_{CO}$, the resistivity shows an activated behaviour, with the activation energy approaching a constant value. The temperature dependence of ρ when $T \ll T_{CO}$ is described by the Arrehenius relation ($\rho = \rho_0 \exp^{(E/kT)}$) as well as the polaron transport relation ($\rho/T = \rho_0 \exp^{(W/kT)}$). A somewhat better fit is obtained with the

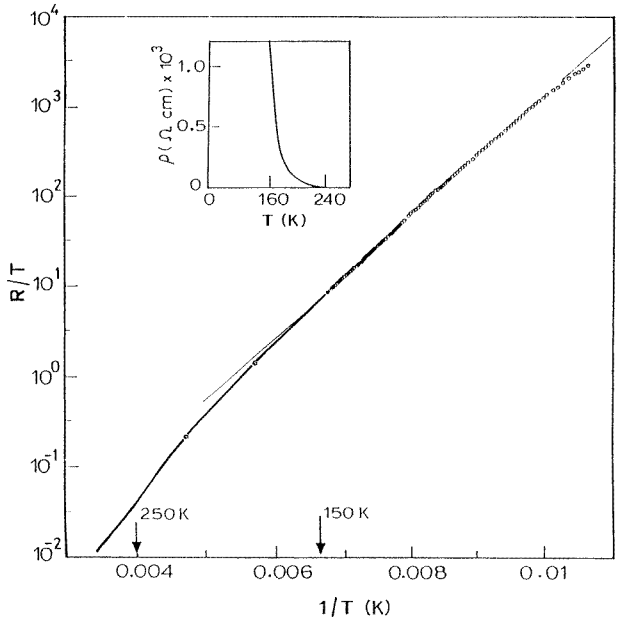

Figure 2. Temperature variation of R/T and the resistivity, ρ, of $Y_{0.5}Ca_{0.5}MnO_3$. R is the resistance.

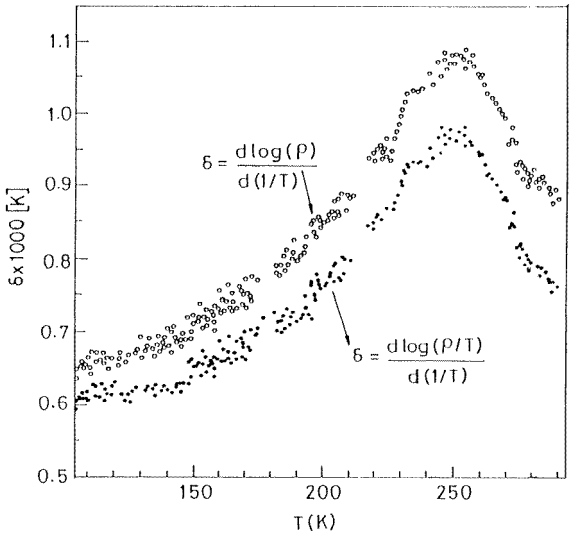

Figure 3. Temperature variation of the derivative δ in $Y_{0.5}Ca_{0.5}MnO_3$. The two curves are for the different relations used for the log derivative as shown (see text).

second relation when the polaron formation energy, W, reaches a constant value of 0.12 eV below 150 K. This can be seen from figure 2 where we have plotted $\log(R/T)$ as a function of $1/T$. We obtain a linear relation when $T < 150$ K, suggesting that the carrier transport is likely to be polaronic in the CO state.

In figure 4 we show the reciprocal of the magnetic susceptibility (χ^{-1}) of $Y_{0.5}Ca_{0.5}MnO_3$ as a function of temperature. The data were obtained in the field-cooled mode at an applied field of 0.2 T. For this field, we find no difference between the FC and ZFC measurements. The data in figure 4 show that χ increases as T is lowered but there is no sign of a sharp magnetic transition. The χ^{-1}–T plot however exhibits certain distinct features and slope changes. The χ^{-1}–T graph shows four clear regions. The first one (marked (1) in the graph) occurs at the highest temperatures where there is a Curie–Weiss behaviour with a Curie temperature, θ_C of 20 K, showing the predominance of a small net ferromagnetic (FM) interaction. Around 260 K, there is an onset of an increase in χ^{-1} over the Curie–Weiss plot. This manifests as a slope change and a dip in the derivative $\mathrm{d}(\chi^{-1})/\mathrm{d}T$ as shown in the inset of figure 4. The second region occurs for $T < 240$ K where the Curie–Weiss law is approximately followed in the 200 K $> T >$ 140 K range with $\theta_C \approx -25$ K, indicating a small net antiferromagnetic (AFM) interaction below the charge-ordering transition. Around 130 K, there is an increase in χ^{-1} or a decrease in χ, resulting in a turn around in the $\mathrm{d}(\chi^{-1})/\mathrm{d}T$ curve. This feature is shown as region (3) in the graph in figure 4. Below 50 K, the Curie–Weiss behaviour is associated with a small negative θ_c. It appears that while there is no long-range ferromagnetic or antiferromagnetic order, the local short-range ordering gives rise to distinct features in the $\mathrm{d}(\chi^{-1})/\mathrm{d}T$ curve. An indication of the presence of a short-range AFM correlation of spins is obtained from the EPR data shown in figure 5 where the line width (ΔH) of the EPR line is plotted against temperature. The line width does not show any perceptible change at $T_{CO} \approx 260$ K, but there is a drop around 135 K. The onset of line narrowing occurs around the same temperature where we see a dip in the magnetic susceptibility (see figure 4).

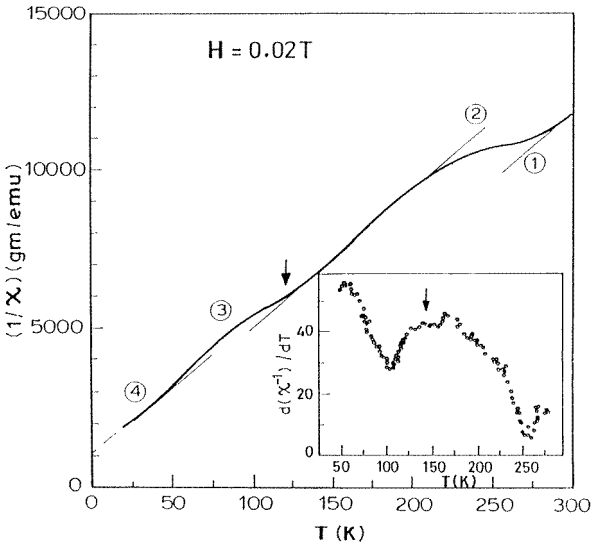

Figure 4. Temperature variation of the magnetic susceptibility of $Y_{0.5}Ca_{0.5}MnO_3$. The inset shows the derivative $d(\chi^{-1})/dT$.

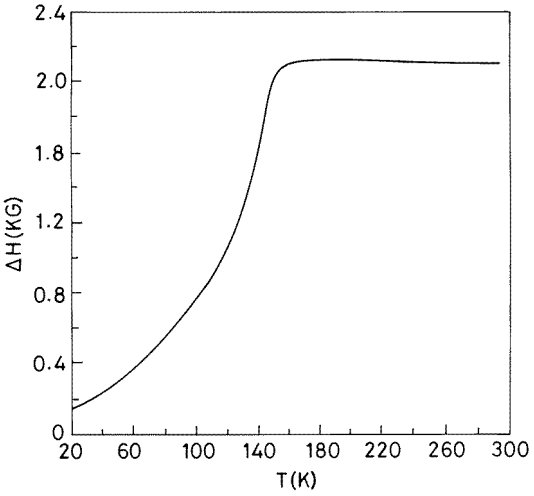

Figure 5. Temperature variation of the EPR line width of $Y_{0.5}Ca_{0.5}MnO_3$.

The absence of long-range magnetic order in $Y_{0.5}Ca_{0.5}MnO_3$ is also evidenced from magnetization measurements. The magnetization of the system shows onset of irreversibility (difference between the FC and ZFC magnetization) when the sample is cooled below 100 K as shown in figure 6. At a measuring field of 0.005 T, a marked difference between the FC and ZFC magnetization (referred to as M_{FC} and M_{ZFC} respectively) is observed around 120 K. While the M_{ZFC} shows a sign of saturation at 20 K, M_{FC} continues to increase. At this temperature, the M_{FC}/M_{ZFC} ratio is greater than 3. At a higher measuring field (0.03 T), the difference between M_{FC} and M_{ZFC} is considerably smaller, becoming measurable only at low temperatures. For a measuring field $\geqslant$0.2 T, $M_{FC} \approx M_{ZFC}$ for

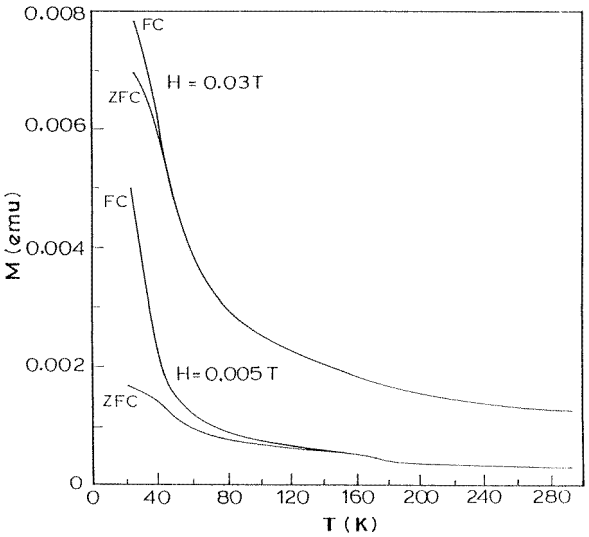

Figure 6. Temperature variation of the magnetization (FC and ZFC) of $Y_{0.5}Ca_{0.5}MnO_3$ at two different measuring fields.

all T. This implies that whatever the cause of the irreversibility, the anisotropy field (which freezes the spins) is not large. The rise of M_{FC} at the lowest T has been observed in several manganates with low $\langle r_A \rangle$ such as $Nd_{0.5}Ca_{0.5}MnO_3$ which do not show a clear transition to the AFM state [9]. It is possible that the onset of irreversibility below 120 K is due to the canted nature of spins or to the random freezing of spins.

As $Y_{0.5}Ca_{0.5}MnO_3$ is cooled, the c parameter contracts more prominently compared to the a and b parameters. From 290 to 120 K, the a to b ratio remains constant around $\sim$1.036 with a maximum deviation of $\pm$0.1%, which is of the same order as the uncertainty in our lattice constants. The change in the a and b parameters in this temperature range is $<$1%, but the c parameter changes by $\sim -8\%$. This large contraction in the c parameter introduces a large orthorhombic distortion. It is to be noted that the change in the c parameter is gradual through the T_{CO} and becomes more prominent below 160 K. In $Pr_{0.7}Ca_{0.3}MnO_3$ there is a small change in the unit cell parameters and volume at T_{CO} which is followed by a continuous change down to the AFM transition at much lower temperature [12]. In $Nd_{0.5}Sr_{0.5}MnO_3$ where the manganate transforms from a metallic FM state to an AFM–CO state ($T_N \approx T_{CO}$), the lattice distortion occurs sharply at T_{CO}. A comparison with $Y_{0.5}Ca_{0.5}MnO_3$ suggests that the factors controlling the CO transition in these two manganates are clearly different [13].

We can quantify the orthorhombic lattice distortion in terms of the dimensionless index D which is defined as $D = \sum_{i=1}^{3} |a_i - a|/3a_i$ where $a_1 = a$, $a_2 = b$ and $a_3 = c/\sqrt{2}$ and $a = (abc/\sqrt{2})^{1/3}$. In figure 7(a), we show the variation of D in $Y_{0.5}Ca_{0.5}MnO_3$ with temperature. It is noteworthy that D in $Y_{0.5}Ca_{0.5}MnO_3$ is considerably larger than in $La_{0.5}Ca_{0.5}MnO_3$ and $Nd_{0.5}Ca_{0.5}MnO_3$ where it is just around 1% at 100 K. In $Y_{0.5}Ca_{0.5}MnO_3$, D is 1.7% at 300 K and increases to 1.75% at 250 K; it remains nearly constant down to $\sim$160 K and again increases to 1.82% at 100 K. This observation confirms the presence of large lattice distortion at room temperature ($T > T_{CO}$) which continues down to low temperatures.

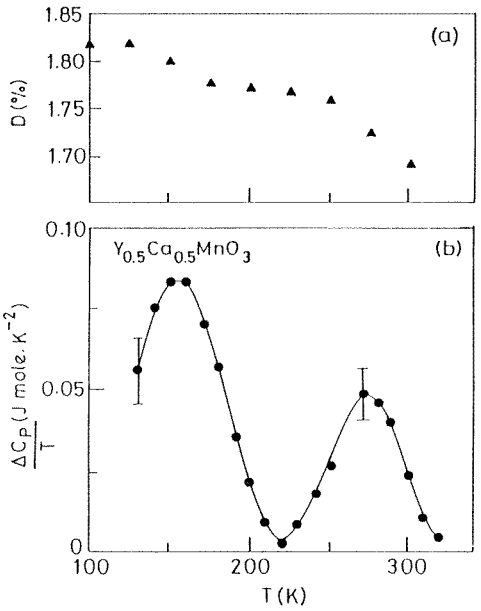

Figure 7. (a) Temperature variation of the lattice distortion index D in $Y_{0.5}Ca_{0.5}MnO_3$. (b) Temperature variation of the excess specific heat ($\Delta C_p/T$) of $Y_{0.5}Ca_{0.5}MnO_3$. The excess specific heat was obtained after subtracting the lattice part. The error bar represents the uncertainty in subtracting the background (see text). The full curve is drawn as a guide to the eye.

In figure 7(b) we present the specific heat data as a function of temperature. The specific heat data are shown as $\Delta C_p/T$ where ΔC_p is the excess specific heat after the subtraction of the lattice part. The subtraction of the lattice part is not unique and introduces some uncertainty in determination of ΔC_p. In the figure, we have shown the uncertainty as an error bar. For the subtraction of the lattice part, we followed the procedure of [8] noting that the excess specific heat $\Delta C \rightarrow 0$ for $T < 100$ K and $T > 320$ K. The lattice contribution was estimated from the interpolation of the specific heat data for $T < 100$ K and $T > 320$ K. The lattice contribution for $T > 50$ K was fitted to an Einstein model with optical frequencies at 180, 550 and 850 K. Two distinct transitions are seen in the specific heat data so obtained, one around 265 K and another around 160 K. The 265 K peak is most likely associated with the CO transition. The value of $\Delta C_p/T$ and the total entropy contained within this specific heat feature (area under the curve) are similar to that in systems like $La_{0.35}Ca_{0.65}MnO_3$ where the CO transition occurs at 265 K. The total entropy (ΔS_{CO}) contained within the peak in $Y_{0.5}Ca_{0.5}MnO_3$ is around 2.5 J mol^{-1} K^{-1} while ΔS_{CO} in $La_{0.35}Ca_{0.65}MnO_3$ is 2.2 J mol^{-1} K^{-1}. These are both about half of $\Delta S \approx R \ln 2$, expected in an order–disorder transformation. The entropy associated with the transition at 160 K is $\sim$4 J mol^{-1} K^{-1}. It seems that this entropy change may be related to the large lattice distortion occurring at this temperature, although part of the contribution could be from local AFM ordering.

A magnetic field of 6 T has negligible effect on the resistivity of $Y_{0.5}Ca_{0.5}MnO_3$ and the magnitude of magnetoresistance does not exceed 10% even in the 100 K region (figure 8). In contrast, $Nd_{0.5}Ca_{0.5}MnO_3$, with a larger $\langle r_A \rangle$ of 1.171 Å, shows considerable change in

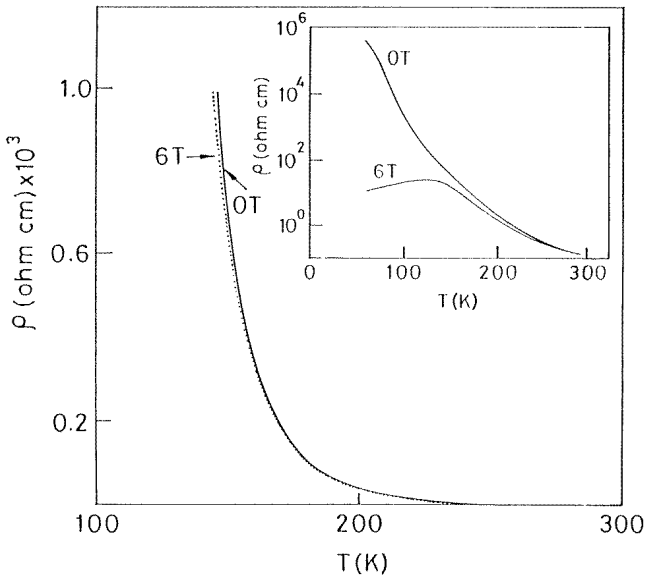

Figure 8. Effect of magnetic field (6 T) on the resistivity of $Y_{0.5}Ca_{0.5}MnO_3$.

the resistivity at 6 T as can be seen from the inset of figure 8 [9, 14]. While it is possible that the charge-ordered state in $Y_{0.5}Ca_{0.5}MnO_3$ may melt at higher magnetic fields ($\gg$6 T), it is noteworthy that it is considerably more stable against magnetic fields compared to $Nd_{0.5}Ca_{0.5}MnO_3$. The present study thus distinguishes two types of charge-ordering in the manganates depending on $\langle r_A \rangle$, the small $\langle r_A \rangle$ regime showing less sensitivity of the CO state to magnetic fields [13].

A distinct charge-ordering gap (Δ_{CO}) in the density of states (DOS) at the Fermi level has been observed in $Nd_{0.5}Sr_{0.5}MnO_3$ at the charge-ordering transition around 150 K [11]. This gap has been measured by vacuum tunnelling spectroscopy. Below T_{CO}, the gap rises rapidly as T decreases and at $T/T_{CO} \leqslant 0.6$, reaches a limiting value of $\approx$0.27 eV (figure 10). We have carried out similar gap measurements on $Y_{0.5}Ca_{0.5}MnO_3$. The experiment was carried out by using a Pt/Rh tip in a cryo-pumped high vacuum environment. The tunnelling current was first stabilized at a high bias ($\approx$2.5 V) using a feedback loop which is much larger than the expected gap Δ_{CO}/e. After stabilization, the feedback voltage was kept at a hold mode and a series of I–V curves recorded digitally. This procedure was repeated on different areas of the sample. An I–V curve of the type shown in figure 9 is obtained by averaging the stored data. The dynamic conductance ($G = \mathrm{d}I/\mathrm{d}V$) obtained numerically from the averaged I–V curve is shown in figure 9. Since $Y_{0.5}Ca_{0.5}MnO_3$ has a high value of resistivity, particularly at low T, tunnelling experiments have to be carried out with care. We did not carry out tunnelling measurements below 200 K because the resistivity was in excess of 40 Ω cm. The high resistivity makes the tunnelling data noisy. Nevertheless, a clear identification of the charge-ordering gap is possible from the tunnelling data. The gap slowly builds up over a temperature range starting from 300 K and saturates below T_{CO}. The value of the gap is $\approx 0.5 \pm 0.05$ eV for $T < T_{CO}$ (figure 10). At higher temperatures ($\approx$300 K), the gap is around 0.2 eV. The value of the gap in $Nd_{0.5}Sr_{0.5}MnO_3$ in the charge-ordered state is much smaller and rises sharply from zero at T_{CO}, in contrast to the gradual change in $Y_{0.5}Ca_{0.5}MnO_3$ (see figure 10).

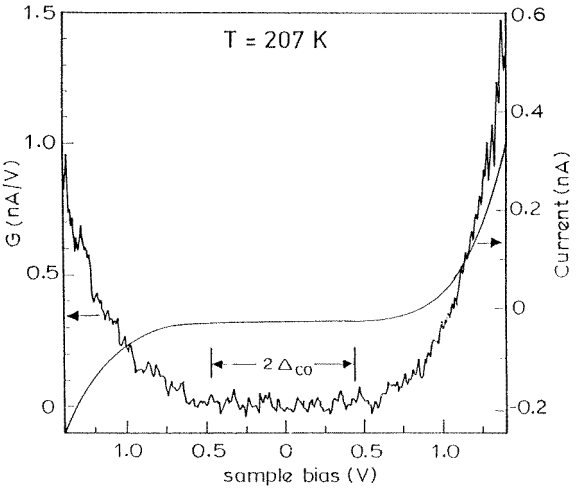

Figure 9. Vacuum tunnelling curves (I–V and $G = \mathrm{d}I/\mathrm{d}V$–$V$) for $Y_{0.5}Ca_{0.5}MnO_3$ at 207 K.

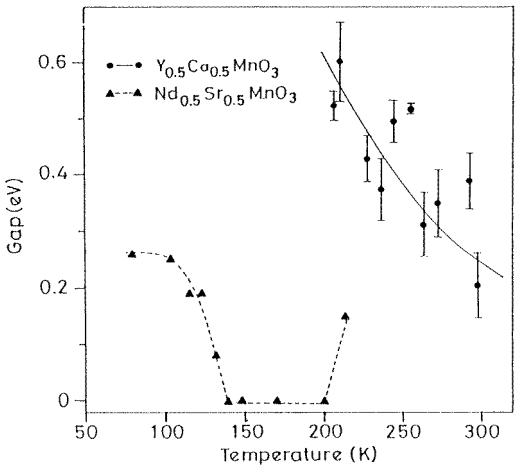

Figure 10. Variation of the charge-ordering gap with temperature in $Y_{0.5}Ca_{0.5}MnO_3$ (filled circles) and $Nd_{0.5}Sr_{0.5}MnO_3$ (filled triangles). The solid and broken lines are guides to the eye. The error bars for $Nd_{0.5}Sr_{0.5}MnO_3$ are of the order of the symbol size.

It is noteworthy that Δ_{CO} in $Y_{0.5}Ca_{0.5}MnO_3$ is much larger than the gap from transport measurements. The value of the transport gap is nearly the same above and below T_{CO} ($\sim$0.13 eV). There is a slope change in the resistivity which shows up as a peak in the derivative δ near T_{CO} (see figure 3). The charge-ordering gap, on the other hand, opens up distinctly below T_{CO}. The large difference between Δ_{CO} and the transport gap below T_{CO} would imply that there are localized states in the gap which take part in conduction. The large value of the measured Δ_{CO} implies that the energy is associated with the charge-ordering process is large. It is likely that the energy associated with charge-ordering, responsible for its stability against the applied magnetic field, arises from the strong co-operative Jahn–Teller distortion. It is noteworthy that in the manganates with small $\langle r_A \rangle$ (as in $Y_{0.5}Ca_{0.5}MnO_3$), the CO transition is often not accompanied by a proper long-range

AFM ordering. The AFM ordering, if occurs at all, has a $T_N \ll T_{CO}$. It is possible that the strong lattice distortion is not homogeneous and the randomness associated with the distortion introduces frustration. In table 1, we have summarized the important properties of $Y_{0.5}Ca_{0.5}MnO_3$ for the purpose of convenience.

Table 1. Important properties of $Y_{0.5}Ca_{0.5}MnO_3$.

Lattice parameters	$a = 5.305$ Å, $b = 5.495$ Å, $c = 7.445$ Å
Orthorhombic distortion index	$D = 1.7\%$ at 300 K
Charge-ordering transition temperatures	
from resistivity data	260 K
from magnetic susceptibility data	260 K
from specific heat data	265 K[a]
Onset of short-range AFM order	130–135 K
Charge-ordering gap	0.2 eV at 300 K
	0.5 eV at 200 K

[a] Broad feature.

To summarize, we have studied charge-ordering in $Y_{0.5}Ca_{0.5}MnO_3$ using different probes (table 1). This material has the smallest $\langle r_A \rangle$ ($\approx$1.128 Å) of all the manganates studied hitherto. Charge-ordering in this manganate occurs in the insulating, paramagnetic state with a high transition temperature ($T_{CO} \sim 260$ K). The charge-ordered state in this manganate is highly stable against the application of a magnetic field ($H \leqslant 6$ T). A strong lattice distortion as well as a large gap are associated with charge-ordering.

Acknowledgments

The authors want to thank Professor S V Bhat for the EPR measurements. We thank the Department of Science and Technology, Government of India and the CSIR (India) for support of this research.

References

[1] Tokura Y, Kuwahara H, Moritomo Y, Tomioka Y and Asamitsu A 1996 *Phys. Rev. Lett.* **76** 3184
Tokura Y, Tomioka Y, Kuwahara H, Asamitsu A, Moritomo Y and Kasai M 1996 *J. Appl. Phys.* **79** 5288
[2] Rao C N R, Cheetham A K and Mahesh R 1996 *Chem. Mater.* **8** 2421
[3] Millis A J, Littlewood P B and Shraiman B I 1995 *Phys. Rev. Lett.* **74** 5144
[4] Röder H, Zang J and Bishop A R 1996 *Phys. Rev. Lett.* **76** 1356
[5] Kuwahara H, Tomioka Y, Asamitsu A, Moritomo Y and Tokura Y 1995 *Science* **270** 961
[6] Lees M R, Barratt J, Balakrishnan G, Mck Paul D and Yethiraj M 1995 *Phys. Rev. Lett.* B **52** 14 303
[7] Tomioka Y, Asamitsu A, Moritomo Y, Kuwahara H and Tokura Y 1995 *Phys. Rev. Lett.* **74** 5108
[8] Ramirez A P, Schiffer P, Cheong S W, Chen C H, Bao W, Palstra T T M, Gammel P L, Bishop D J and Zegarski B 1996 *Phys. Rev. Lett.* **76** 3188
[9] Vogt T, Cheetham A K, Mahendiran R, Raychaudhuri A K, Mahesh R and Rao C N R 1996 *Phys. Rev.* B **54** 15 303
[10] Biswas A and Raychaudhuri A K 1996 *J. Phys.: Condens. Matter* **8** L739
[11] Biswas A, Raychaudhuri A K, Mahendiran R, Mahesh R and Rao C N R 1997 *J. Phys.: Condens. Matter* **9** L355
[12] De Teresa J M, Ibarra M R, Marquina C, Algarabel P A and Oseroff S 1996 *Phys. Rev.* B **54** 12 689
[13] Kumar N and Rao C N R 1997 *J. Solid State Chem.* **129** 363
[14] Mahendiran R, Mahesh R, Gundakaram R, Raychaudhuri A K and Rao C N R 1996 *J. Phys.: Condens. Matter* **8** L455